

Analysis of buried ink elements in library artefacts using pulsed thermography

Giovanni Caruso¹, Noemi Orazi², Stefano Paoloni², Ugo Zammit², Fulvio Mercuri²

¹ Institute of Heritage Science, Italian National Research Council, via Salaria km 29,300, 00015 Monterotondo Stazione, Italy

² Department of Industrial Engineering, University of Rome Tor Vergata, via Politecnico 1, 00133 Roma, Italy

ABSTRACT

Pulsed thermography is a well-established method for the non-destructive analysis of cultural heritage items. This technique has been recently applied by the authors of this paper for reading written scraps, used for the making of bookbinding of ancient manuscripts, located between the end papers and the covers. The readability of the hidden text depends on several geometrical, optical and thermal parameters characterizing the typology of paper and the ink employed. To this end, a comprehensive mathematical model was developed by the authors for analyzing the influence of the various involved parameters. In particular, two indices were introduced, namely the signal contrast and the distortion index, used to quantitatively characterize the hidden text readability. Several numerical simulations are reported for assessing the dependence of the contrast and distortion from various parameters appearing in the model. Finally, a preliminary application to the analysis of original books is also presented.

Section: RESEARCH PAPER

Keywords: pulsed thermography; mathematical modelling; hidden text; readability; measurement

Citation: G. Caruso, N. Orazi, S. Paoloni, U. Zammit, F. Mercuri, Analysis of buried ink elements in library artefacts using pulsed thermography, Acta IMEKO, vol. 13 (2024) no. 3, pp. 1-7. DOI: [10.21014/actaimeko.v13i3.1840](https://doi.org/10.21014/actaimeko.v13i3.1840)

Section Editor: Fabio Leccese, Università Degli Studi Roma Tre, Rome, Italy

Received March 6, 2024; **In final form** April 8, 2024; **Published** September 2024

Copyright: This is an open-access article distributed under the terms of the Creative Commons Attribution 3.0 License, which permits unrestricted use, distribution, and reproduction in any medium, provided the original author and source are credited.

Corresponding author: Giovanni Caruso, e-mail: giovanni.caruso@cnr.it

1. INTRODUCTION

Among the non-destructive investigation techniques, infrared thermography is nowadays well-established for the evaluation of thermophysical parameters [1] and for performing tests in industrial [2], [3] and cultural heritage items [4], [5]. In this regard, more recently, it has been applied for the examination of different kind of artworks, for obtaining important information about their structure and, in general, for increasing their knowledge, assessing their maintenance conditions, and possibly for evaluating a possible restoration. Among its various configurations, the pulsed thermography is an effective tool [6], [7], [8] which can be successfully applied to perform a depth-resolved analysis of a wide variety of features in artifacts. For example, it has been revealed useful for the analysis of ancient bronzes [9], [10], wooden/canvas paintings [11]-[13], frescos [14], [15], or historic buildings [16]. Recently it has also been applied to the investigation of ancient books [17]. This technique is simple but quite powerful. The working principle [18] relies on exciting the sample with a flash of visible light which can be absorbed in correspondence of the specimen surface (case of optically opaque samples) or inside its volume (case of optically

semi-transparent samples) and converted into heat. The heat can diffuse in the sample volume and induce a temperature increase implying a variation of the infrared emission which is detected by an infrared camera (Figure 1a shows the setup employed in this study). In the case of optically opaque samples, the camera can detect only the infrared radiation emitted by the sample surface, whereas in the case of optically semi-transparent samples, the infrared image recorded by the camera is contributed also by the emission relevant to the layers beyond the surface. The infrared image can reveal features lying beyond the illuminated surface if they constitute a discontinuity in the thermal and optical properties of the sample. In particular, pulsed thermography provides depth-resolved investigations since features located at different depths appear in the infrared image with different time delays. Such a possibility is not granted by most of the other techniques employed in the cultural heritage field such as infrared reflectography [19].

Recently the authors of this paper successfully applied pulsed thermography for the detection of writings belonging to scraps of earlier manuscripts and parchments, used to realize the bookbinding of ancient books [20], [21]. The buried text can be

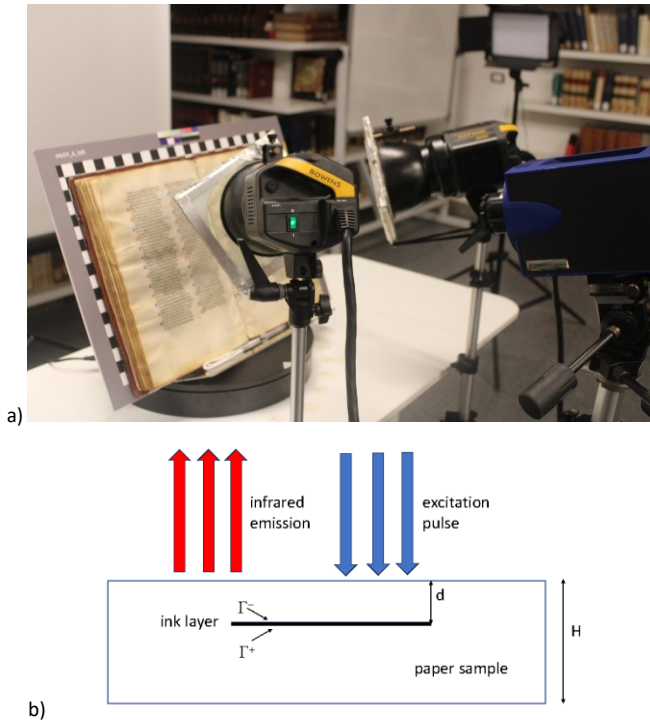


Figure 1. a) Set up of the thermographic system; b) Schematic representation of the specimen considered in the mathematical model.

revealed because of two different effects: on one hand, the ink has a different emissivity with respect to surrounding paper (optical effect); on the other hand, the ink absorbs visible light more than the surrounding paper, inducing a larger temperature increase and a consequent increase of infrared radiation (thermal effect). Compared to infrared reflectography, pulsed thermography has been proven to enable more effective detection of hidden graphical features, especially when buried below optically diffusing layers such as paper leaves [22]. In addition, unlike reflectography, pulsed thermography can also offer the possibility to distinguish between features located at different depth levels.

In this paper, a comprehensive mathematical model is recalled, for the description of the infrared emission of a sample made of an optically semi-transparent material and containing an ink layer buried inside at a certain depth beyond the front surface, upon excitation with a pulse of visible light. The model is three-dimensional and takes into account lateral diffusion of the heat generated in the ink layer after absorption of the light pulse.

A finite element scheme is developed based on the proposed model, and it is used to perform numerical simulations of the investigated phenomenon. In particular, the reported simulations are designed to investigate on the factors affecting the readability of the buried text. To this end two indices are introduced for quantitatively evaluating this property, namely the signal contrast and the signal distortion. The former is the difference of the infrared signal in correspondence of the ink layer and far away from it, whereas the latter, related to the blurring of the ink infrared image, measures how much the signal contrast along a segment perpendicularly crossing the ink layer deviates from the step-like profile.

The numerical results show that the signal contrast exhibits a maximum just after the flash pulse for small to moderate ink depths, since in those cases the direct infrared emission of the ink prevails in the generation of the ink infrared image. For larger value of the depth the signal contrast reaches a maximum at later

times since in those cases the thermal contribution is dominant in the signal generation.

The distortion increases with time since it essentially depends on the lateral diffusion of the heat generated in the ink layer. On the other hand, it has a negligible dependence on the depth of the ink layer, i.e. if one compute the distortion index for an ink layer buried at different depths, it will be very similar in all cases at each fixed time delay from the flash pulse.

Finally, some experimental results are shown, regarding the detection of a hidden text buried beneath the end-leaves of an ancient manuscript. The experimental results show the effectiveness of the pulsed thermography for this application and are in qualitative agreement with the theoretical considerations.

The paper is organized as follows: in Section 2 the mathematical model is presented and the mathematical assumptions at the basis of the model are mentioned. Moreover, the numerical method employed for performing the numerical simulations is described. In Section 3 the numerical results are reported. In Section 4 the apparatus used to perform the experiments is described and the experimental results are depicted. In Section 5 both the numerical and experimental results previously reported are discussed and some general considerations are formulated. Finally, in Section 6 the main conclusions concerning the present work are pointed out.

2. MODEL

In this section the mathematical model used for performing all the numerical simulations reported in the paper will be briefly recalled.

In Figure 1b a schematic representation of the specimen considered in the model is reported. It is composed of a paper layer of lateral dimension A, B and thickness H with an ink layer of lateral dimensions a, b and thickness b , buried inside the paper at a certain depth d . A cartesian frame is introduced, with origin in the centre of the paper illuminated surface, with axes $(x, y) = \bar{x}$ parallel to the lateral sides of the specimen and z directed downward along the thickness. The specimen is excited by a pulse of visible light of uniform intensity I_0 and the consequent variation of infrared radiation is computed as a function of the position \bar{x} and time t . By assuming $b \ll H$, a concentration of capacity is operated for the ink layer which is thus modelled as a surface domain whereas the paper domain is three dimensional. By indicating with $T_p(\bar{x}, z, t)$ the temperature inside the paper domain and with $T_i(\bar{x}, t)$ the temperature inside the ink layer, the field equation governing the temperature evolution can be written as

$$\begin{aligned} \rho_p c_p \frac{\partial T_p}{\partial t} - k_{p\bar{x}} \Delta_{\bar{x}} T_p - k_{pz} \frac{\partial T_p}{\partial z} &= f_p \\ h \rho_i c_i \frac{\partial T_i}{\partial t} - h k_i \Delta_{\bar{x}} T_i &= f_i. \end{aligned} \quad (1)$$

In equation (1), ρ , c , and k indicate, respectively, the volume density, the specific heat, and the heat conductivity, with subscript p and i referring, respectively, to quantities relevant to the paper domain and to the ink domain. In particular, an anisotropic heat diffusion was accounted for in the paper, with planar heat conductivity $k_{p\bar{x}}$, and vertical heat conductivity k_{pz} . Finally, f is the heat source term and $\Delta_{\bar{x}}$ is the Laplacian operator acting only along the planar coordinates. In order to compute the expression for the heat source terms, it is assumed that the excitation light pulse undergoes infinite reflections at the paper

front and rear surfaces, and a concentrated absorption when crossing the ink layer. By generalizing an expression given in [23] in the case of a uniform optically semi-transparent specimen, the spatial profile $I(\bar{x}, z)$ of the light intensity inside the specimen in the region containing the ink layer is given by:

$$I(\bar{x}, z) = \frac{I_0(1-R)}{1-e^{-2\alpha H R^2 \gamma^2}} e^{-\alpha z} + \frac{I_0(1-R)e^{-2\alpha H R \gamma^2}}{1-e^{-2\alpha H R^2 \gamma^2}} e^{\alpha z} \quad 0 < z < d$$

$$I(\bar{x}, z) = \frac{I_0(1-R)\gamma}{1-e^{-2\alpha H R^2 \gamma^2}} e^{-\alpha z} + \frac{I_0(1-R)e^{-2\alpha H R \gamma}}{1-e^{-2\alpha H R^2 \gamma^2}} e^{\alpha z} \quad d < z < H,$$
(2)

where R is the reflection coefficient, γ is the transmission coefficient of the ink layer and α is the light absorption coefficient of the paper.

It can be noticed that $I(\bar{x}, z)$ is discontinuous across $z = d$, and its jump is equal to the light absorbed by the ink layer.

A similar expression holds in the region non containing the ink layer, by setting $\gamma = 1$ in (2). Needless to say that in this case $I(\bar{x}, z)$ is continuous along the paper thickness. The temporal dependence of I is a dirac mass centered at the time of the flash pulse.

The expression of the source terms in (1) reads as:

$$f_p(\bar{x}, z, t) = -\chi \frac{\partial I(\bar{x}, z)}{\partial t} \delta(t)$$

$$f_i(\bar{x}, z) = -[I(\bar{x}, z)]_{z=d} \delta(t) + \left. \frac{\partial T_p}{\partial z} \right|_{\Gamma^+} - \left. \frac{\partial T_p}{\partial z} \right|_{\Gamma^-},$$
(3)

where χ is the fraction of light effectively converted into heat (the remaining is scattered away), Γ^+ and Γ^- are, respectively, the interfaces between the ink layer and surrounding paper for $z = d^+$ and $z = d^-$, $\delta(t)$ is the Dirac mass centered at $t = 0$ and $[\cdot]_d$ denotes the jump of the function inside the brackets across $z = d$.

The infrared signal S recorded by the camera is given by:

$$S(\bar{x}, t) = K \left[\int_0^d \beta T_p(\bar{x}, z, t) e^{-\beta z} dz + \eta T_i(\bar{x}, t) e^{-\beta d} + (1-\eta) \int_d^H \beta T_p(\bar{x}, z, t) e^{-\beta z} dz \right]$$
(4)

in the region containing the ink layer, whereas in the region not containing the ink layer the following expression holds:

$$S(\bar{x}, t) = K \int_0^H \beta T_p(\bar{x}, z, t) e^{-\beta z} dz.$$
(5)

In (4) and (5) β is the infrared absorption coefficient in the paper, η is the concentrated emissivity of the ink layer and K is a constant.

In order to perform the numerical simulations shown in the next section, a finite element scheme was developed based on the model previously reported, and a dedicated program in the Matlab environment was written. The finite element scheme employs triangular elements for the mesh of the ink layer and prisms with triangular bases for the mesh of the paper volume, with linear shape functions. The isoparametric map is used to perform the integrals in each element belonging to the mesh. Finally, the Crank-Nicolson algorithm is adopted for the time integration. Alternatively, Comsol could be used to solve the

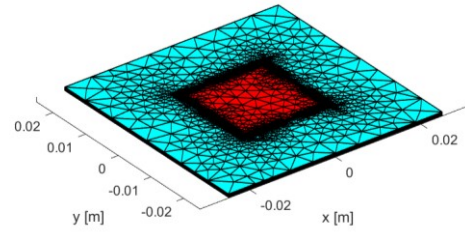


Figure 2. Typical mesh of the considered specimen with a mesh refinement along the lateral sides of the ink layer.

weak formulation of the model equations previously reported, automatically managing all the machinery required by the finite-element method. On the other hand, the methodology adopted here allows one to have direct control on the numerical procedure and is preferable for performing a curve fitting of the experimental results for physical parameter estimation.

A typical mesh of the specimen considered in the model is reported in Figure 2, where a mesh refinement is used near the lateral boundaries of the ink layer in order to accurately evaluate the lateral heat flow and consequently the distortion index of the ink layer.

3. NUMERICAL RESULTS

In this section some numerical results will be reported, aimed at investigating the factors affecting the readability of the buried text.

To this end two indices are introduced, namely the signal contrast $C(\bar{x}, t)$ and the distortion index $D(t)$. The former is defined as:

$$C(\bar{x}, t) = S(\bar{x}, t) - S_\infty(t),$$
(6)

where S_∞ is the signal detected far away from the ink layer, where its behaviour is almost independent from the spatial position. The distortion index $D(t)$ is defined as:

$$D(t) = x_b(t) - x_a(t).$$
(7)

In (7), x_a and x_b are the abscissas along a segment perpendicularly crossing an ink layer side in correspondence of its midspan, where the signal contrast is respectively equal to 98% and 2% of its maximum value (see Figure 3).

All the numerical simulations reported in the foregoing were obtained by using the parameter values in Table 1, which are typical for a standard paper sheet and were carefully estimated by suitable experimental results as described in [21].

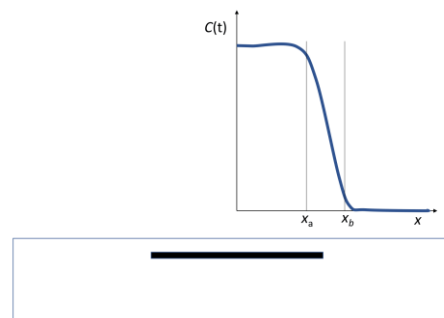


Figure 3. Definition of the distortion index $D(t)$.

Table 1. Parameter values used in the numerical simulations.

Parameter	Value
ρ_p, ρ_i	750 kg/m ³
c_p, c_i	1400 J/(kg K)
k_{pz}, k_i	0.1074 W/(m K)
$k_{p\bar{x}}$	0.1611 W/(m K)
α	$12.81 \times 10^3 \text{ m}^{-1}$
β	$24.01 \times 10^3 \text{ m}^{-1}$
η	0.9
χ	0.065

In Figure 4, the signal contrast computed at the centre of the specimen, location obviously exhibiting the maximum contrast value, versus time is reported in correspondence of different values of the ink layer depth d . The distortion index corresponding to each tested value of depth d is reported in Figure 5, versus the time t .

To highlight more clearly the blurring effect due to the heat lateral diffusion, in Figure 6 the contrast along a segment perpendicularly crossing a lateral side of the ink is reported. Each profile corresponds to a different value of the ink layer depth d , and it was computed at the time for which the contrast at the ink centre is maximum. Accordingly, each profile corresponds to a different time, the greater is the ink layer depth d , the greater is the time at which the contrast in the centre of the ink layer reaches its maximum (Figure 4).

Finally, a simulation was run in order to assess the separate contributions of the thermal and optical effects to the generation of the infrared signal. To this end, in Figure 7 the signal contrast in correspondence of the centre of the ink layer is reported versus the time t .

Two different values of the ink layer depth are considered, and for each depth two curves are reported: one accounting for both the thermal and the optical effects together (complete model) and a second one where only the thermal effect is acting. The latter was obtained by deleting from the infrared signal the direct ink layer emission (i.e. by setting $\eta = 0$ in the second term appearing in (4)).

4. EXPERIMENTAL RESULTS

In this section some experimental results are reported, showing an application of the pulsed thermography for the detection of text buried under the end-leaves of an ancient manuscript.

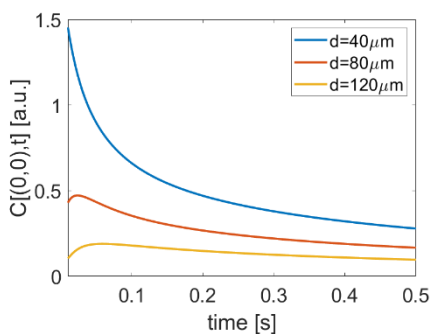


Figure 4. Signal contrast at the centre of the ink layer versus time in correspondence of different values of the ink layer depth.

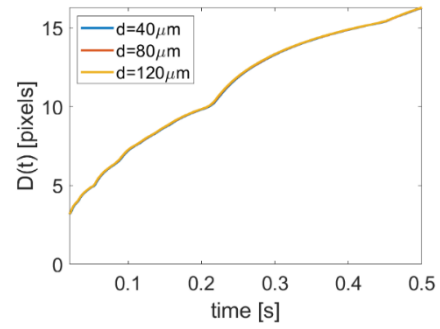


Figure 5. Distortion index versus time in correspondence of different values of the ink layer depth. For the conversion from mm to pixels a pitch value of 100 μm was assumed.

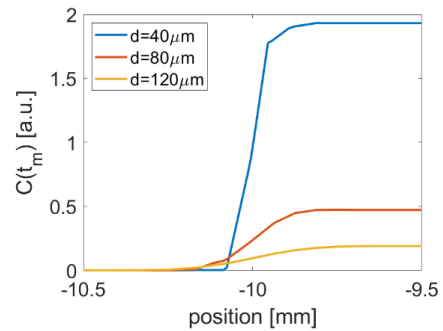


Figure 6. Signal profiles along a segment perpendicularly crossing a lateral side of the ink layer at its midspan, versus position. Several values of ink layer depth considered in the simulation.

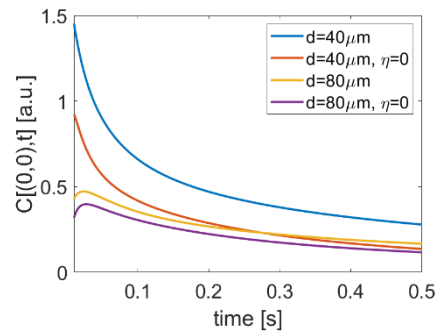


Figure 7. Signal contrast at the centre of the ink layer versus time, in correspondence of different values of the ink layer depth. For each value of the ink layer depth two cases are considered: in one case the complete model was used to run the simulation, in the second case the ink layer infrared emission was excluded.

To this end, the manuscript sample was heated by using two flash lamps symmetrically oriented with respect to the book page to be investigated. The flash duration was approximately equal to 3 ms. Infrared radiation from the flash lamps was cut off by proper filters to prevent their reflection towards the camera so that the signal revealed by the infrared camera is contributed only by the direct emission of the paper sample. A Cedip JADE MWIR camera having a 3.6-5.1 μm wavelength sensitivity range and a focal plane array with 320×240 pixels was used for the acquisition (Figure 1b).

The experimental results presented in the foregoing were obtained by preliminary measurements on an ancient manuscript.

In Figure 8 three thermograms are reported, representing the detection of a hidden text located at almost 100 μm under the surface of the book end paper. In particular, the image a) is recorded 0.02 s after the flash pulse, the image b) 0.04 s after the flash pulse and, finally, the image c) 0.16 s after the flash pulse.

The thermogram collected 0.04 s after the light pulse exhibits the best contrast C but at that time the blurring effect prevents a clear readability of the hidden text. The thermogram recorded after 0.02 s still have a satisfying contrast level together with a reduced blurring effect of the image and is thus preferable for a clear readability of the hidden text. The last thermogram (Figure 8 c) presents a low contrast with a high distortion index, so the readability of the hidden text is quite difficult.

Finally, in Figure 9 the experimental thermographic signal is reported, along a segment perpendicularly crossing an ink letter across its boundary. The blurring effect clearly appears and it is in qualitatively agreement with the numerical contrast profiles reported in Figure 6.

5. DISCUSSION

The numerical results reported in the previous section were performed in order to investigate the readability of hidden text in ancient manuscripts, in terms of the signal contrast C and the signal distortion D . First, the influence of the ink layer depth d is investigated, which turned out to be crucial for the text readability.

The contrast curves reported in Figure 4 relevant to different values of the ink layer depth d exhibit different behaviours. In particular, the contrast at any fixed time after the flash pulse increases with the decrease of d . For $d = 40 \mu\text{m}$ the contrast reaches a maximum just after the flash pulse, and after that monotonically decreases with time. In fact, the depth d is so small that the heat generated inside the ink due to the light absorption induces a maximum radiation soon after the flash pulse. By increasing the time, the heat generated inside the ink diffuses in the layers beyond the ink and thus the infrared radiation due to the ink decreases. A different behaviour is exhibited by the curves relevant to $d = 80 \mu\text{m}$ and $d = 120 \mu\text{m}$, where the signal

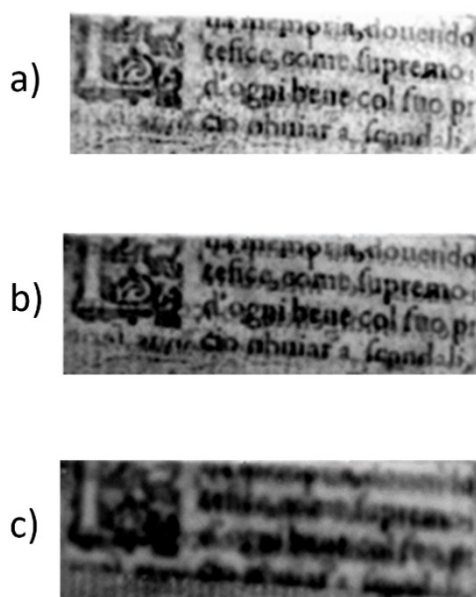


Figure 8. Experimental infrared image of a buried text in the **end-leaf** of an ancient **manuscript** taken at different time delays from the flash pulse.

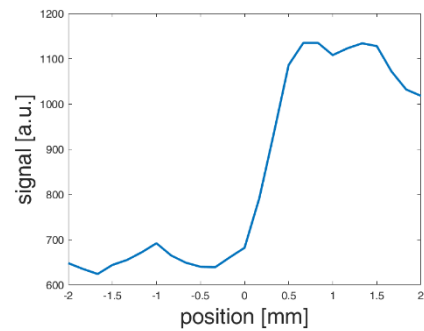


Figure 9. Experimental signal profile along a segment perpendicularly crossing the border of an ink letter of a buried text in the end-leaves of an ancient manuscript.

contrast reaches a maximum at a certain time delay t_m after the flash pulse. In particular, t_m turns out to increase with the increase of d . This is because the infrared emission in the region where the ink layer is located is largely attenuated by the absorption in the layers above the ink. Accordingly, in order to get an increase of the signal contrast revealed by the infrared camera, the heat generated in the ink layer after absorption of the light pulse must diffuse upward inducing a temperature increase and a consequent increase of infrared emission in the layers close to the specimen front surface. Obviously, the greater is d , the greater will be the time needed by the diffusion to produce a temperature increase in the volume where the consequent infrared emission can reach the camera.

In order to assess the contribution to the detected infrared signal due to the thermal and optical effect the numerical simulations reported in Figure 7 were performed. By considering the two values of ink layer depth $d = 40 \mu\text{m}$ and $d = 80 \mu\text{m}$, one simulation was performed by considering the complete model (both effects acting at the same time), whereas a second simulation was run by neglecting the direct infrared emission operated by the ink layer (so only the thermal effect is contributing to the signal generation). The results show that for the considered values of d both the effects are important for the generation of the signal contrast. As expected, if the value of d is small the direct emission of the ink layer becomes important since it is poorly attenuated by volume absorption in the volume above the ink layer. On the other hand, for greater values of d the thermal effect becomes predominant in the signal contrast generation since the direct emission operated by the ink layer is almost totally absorbed before exiting the specimen.

The distortion index relevant to the three values of d considered in the simulations reported in Figure 4, is depicted in Figure 5 versus the time t . As it clearly appears, for each fixed time t after the flash pulse the distortion index is not affected by the ink layer depth d . This result shows that the blurring effect of the revealed ink layer image depends only on the lateral diffusion of the thermal heat initially generated into the ink layer upon light pulse absorption, and thus monotonically increases with the time.

In order to better highlight the behaviour of the blurring effect in Figure 6 the signal contrast is depicted along a segment perpendicularly crossing the ink layer in correspondence of the midspan of a lateral side. Each of the three curves is relevant to a different value of the ink layer depth d , and it is computed at the time t_m where the signal contrast reaches a maximum at that value of d (see Figure 4). It clearly appears that for small values of d it is possible to have the best readability soon after the flash

pulse, when the signal contrast is maximum and the distortion index is very small. In fact the curve relevant to $d = 40 \mu\text{m}$ in the figure exhibits a very high contrast with an almost step-like behaviour. For larger values of d the distortion index at the time t_m (when the maximum contrast was reached) can be important, increasing with the increase of d and, consequently, of t_m . In those cases it is convenient, in order to achieve the best readability of the buried text, to consider thermograms at a time shorter than t_m , when the signal contrast is already satisfying and the image blurring is still acceptable. These considerations are qualitatively confirmed by the experimental images reported in Figure 8, representing the detection of a text buried under the end-leaves of an ancient manuscript.

6. CONCLUSIONS

In this paper the innovative use of pulsed thermography for reading hidden text contained in ancient manuscripts is considered.

A detailed mathematical model was developed for quantitatively assessing the readability of the hidden text, accounting for three-dimensional heat diffusion inside the specimen. Two indices for measuring the text readability were introduced: the signal contrast C and the distortion index D .

Several numerical results were presented, assessing the influence of the main factors involved in the phenomenon. In particular, the signal contrast at each fixed time after the flash pulse is greatly affected by the ink layer depth d , and is larger for smaller values of d . It attains a maximum at a certain delay t_m after the flash pulse, with t_m increasing with d .

On the other hand, the distortion index measuring the blurring effect of the detected image turned out to depend solely on the time, since it is affected by the heat lateral diffusion. In particular, it monotonically increases with time and is independent of d at any fixed time t . As a consequence, for small values of d , the best readability is achieved soon after the flash pulse, when the contrast is maximum and the distortion is very low. For larger values of d the best readability is not achieved at t_m since at that time the blurring effect may be consistent, but a shorter time should be considered.

Finally, some experimental results on a real case were also presented, in order to show the effectiveness of the technique.

REFERENCES

- [1] P. Bison, F. Cernuschi, A. Muscio, E. Grinzato, A survey on thermophysical properties assessment, *Quant. Infr. Therm. J.* (2023), pp. 1-13.
DOI: [10.1080/17686733.2023.2215102](https://doi.org/10.1080/17686733.2023.2215102)
- [2] P. Nooralishahi, S. Pozzer, G. Ramos, F. López, X. Maldague, The registration of multi-modal point clouds for industrial inspection, *Quant. Infr. Therm. J.* (2023), pp. 1-18.
DOI: [10.1080/17686733.2023.2232586](https://doi.org/10.1080/17686733.2023.2232586)
- [3] J. Melada, P. Arosio, M. Gargano, N. Ludwig, Automatic thermograms segmentation, preliminary insight into spilling drop test, *Quant. Infr. Therm. J.* (2023), pp. 1-15.
DOI: [10.1080/17686733.2023.2213555](https://doi.org/10.1080/17686733.2023.2213555)
- [4] V. P. Vavilov, P. G. Bison, D. D. Burleigh, Ermanno Grinzato's contribution to infrared diagnostics and nondestructive testing: in memory of an outstanding researcher, *Quant. Infr. Therm. J.* (2023), pp. 1-14.
DOI: [10.1080/17686733.2023.2170647](https://doi.org/10.1080/17686733.2023.2170647)
- [5] D. Gavrilov, R. G. Maev, D. P. Almond, A review of imaging methods in analysis of works of art: thermographic imaging method in art analysis, *Can. J. Phys.* 92(4) (2014), pp. 341-364.
DOI: [10.1139/cjp-2013-0128](https://doi.org/10.1139/cjp-2013-0128)

- [6] S. Paoloni, N. Orazi, U. Zammit, P. Bison, F. Mercuri, A note on the early thermographic approaches for the investigation of the cultural heritage, *Quant. Infr. Therm. J.* (2023), pp. 1-13.
DOI: [10.1080/17686733.2023.2243575](https://doi.org/10.1080/17686733.2023.2243575)
- [7] J. C. Candoré, J. L. Bodnar, V. Detalle, P. Grossel, Non-destructive testing of works of art by stimulated infrared thermography, *Eur. Phys. J. Appl. Phys.* 57(2) (2012), pp. 21002.
DOI: [10.1051/epiap/2011110266](https://doi.org/10.1051/epiap/2011110266)
- [8] C. Ibarra-Castanedo, F. Khodayar, M. Klein, S. Sfarra, X. Maldague, H. Helal, M. Tayoubi, B. Marini, J. C. Barré, Infrared vision for artwork and cultural heritage NDE studies: principles and case studies, *Insight* 59(5) (2017), pp. 243-248.
DOI: [10.1784/insi.2017.59.5.243](https://doi.org/10.1784/insi.2017.59.5.243)
- [9] F. Mercuri, G. Caruso, N. Orazi, U. Zammit, C. Cicero, O. Colacicchi Alessandri, M. Ferretti, S. Paoloni, Interface thermal conductance characterization by infrared thermography: A tool for the study of insertions in bronze ancient Statuary, *Infrared Phys. Technol.* 90 (2019), pp. 31-39.
DOI: [10.1016/j.infrared.2018.02.002](https://doi.org/10.1016/j.infrared.2018.02.002)
- [10] F. Mercuri, N. Orazi, U. Zammit, A. Giuffredi, C. S. Salerno, C. Cicero, S. Paoloni, The manufacturing process of the Capitoline She Wolf: a thermographic method for the investigation of repairs and casting faults, *J. Archaeol. Sci. Rep.* 14 (2017), pp. 199–207.
DOI: [10.1016/j.jasrep.2017.05.051](https://doi.org/10.1016/j.jasrep.2017.05.051)
- [11] M. Pucci, C. Cicero, N. Orazi, F. Mercuri, U. Zammit, S. Paoloni, M. Marinelli, Active infrared thermography applied to the study of a painting on paper representing the Chigi's family tree, *Stud. Conserv.* 60(2) (2015), pp. 88-96.
DOI: [10.1179/2047058413Y.0000000117](https://doi.org/10.1179/2047058413Y.0000000117)
- [12] S. Laureti, S. Sfarra, H. Malekmohammadi, P. Burrascano, D. A. Hutchins, L. Senni, G. Silipigni, X.P.V. Maldague, M. Ricci, The use of pulse-compression thermography for detecting defects in paintings, *NDT and E Int.* 98 (2018), pp. 147–154.
DOI: [10.1016/j.ndteint.2018.05.003](https://doi.org/10.1016/j.ndteint.2018.05.003)
- [13] Y. Liu, F. Wang, K. Liu, M. Mostacci, Y. Yao, S. Sfarra, Deep convolutional autoencoder thermography for artwork defect detection, *Quant. Infr. Therm. J.* (2023), pp. 1-17.
DOI: [10.1080/17686733.2023.2225246](https://doi.org/10.1080/17686733.2023.2225246)
- [14] L. Bodnar, J. C. Candoré, J. L. Nicolas, G. Szatanik, V. Detalle, J. M. Vallet, Stimulated infrared thermography applied to help restoring mural paintings, *NDT E Int.* 49 (2012), pp. 40-46.
DOI: [10.1016/j.ndteint.2012.03.007](https://doi.org/10.1016/j.ndteint.2012.03.007)
- [15] J. Williams, F. Corvaro, J. Vignola, D. Turo, B. Marchetti, M. Vital, Application of non-invasive active infrared thermography for delamination detection in fresco, *Int. J. Therm. Sci.* 171 (2022), art. no. 107185.
DOI: [10.1016/j.ijthermalsci.2021.107185](https://doi.org/10.1016/j.ijthermalsci.2021.107185)
- [16] N. P. Avdelidis, A. Moropoulou, Applications of infrared thermography for the investigation of historic structures, *J. Cult. Herit.* 5(1) (2004), pp. 119–127.
DOI: [10.1016/j.culher.2003.07.002](https://doi.org/10.1016/j.culher.2003.07.002)
- [17] S. Sfarra, M. Regi, M. Tortora, C. Casieri, S. Perilli, D. Paoletti, A multi-technique nondestructive approach for characterizing the state of conservation of ancient bookbindings, *J. Therm. Anal. Calorim.* 132 (2018), pp. 1367-1387.
DOI: [10.1007/s10973-018-6997-1](https://doi.org/10.1007/s10973-018-6997-1)
- [18] K. Blessley, C. Young, J. Nunn, J. Coddington, S. Shepard, The feasibility of flash thermography for the examination and conservation of works of art, *Stud. Conserv.* 55(2) (2010), pp. 107–120.
DOI: [10.1179/sic.2010.55.2.107](https://doi.org/10.1179/sic.2010.55.2.107)
- [19] J. Peeters, G. Steenackers, S. Sfarra, S. Legrand, C. Ibarra-Castanedo, K. Janssens, G. Van der Snickt, IR reflectography and active thermography on artworks: the added value of the 1.5–3 μm band, *Appl. Sci.* 8(1) (2018).
DOI: [10.3390/app8010050](https://doi.org/10.3390/app8010050)
- [20] G. Caruso, F. Mercuri, U. Zammit, S. Paoloni, S. Ceccarelli, N. Orazi, 3D flow effects in the imaging of subsurface graphical features in semi-transparent media by pulsed thermography, *Measurement* 185 (2021), pp. 110111.

- DOI: [10.1016/j.measurement.2021.110111](https://doi.org/10.1016/j.measurement.2021.110111)
- [21] G. Caruso, S. Paoloni, N. Orazi, C. Cicero, U. Zammit, F. Mercuri, Quantitative evaluations by infrared thermography in optically semi-transparent paper-based artefacts, *Measurement* 143 (2019), pp. 258-266.
DOI: [10.1016/j.measurement.2019.04.086](https://doi.org/10.1016/j.measurement.2019.04.086)
- [22] F. Mercuri, S. Paoloni, C. Cicero, U. Zammit, N. Orazi, Infrared emission contrast for the visualization of subsurface graphical features in artworks, *Infrared Physics & Technology* 89 (2018), pp. 223–230.
DOI: [10.1016/j.infrared.2018.01.012](https://doi.org/10.1016/j.infrared.2018.01.012)
- [23] A. Salazar, A. Mendioroz, E. Apinaniz, C. Pradere, F. Noel, J. C. Batsale, Extending the flash method to measure the thermal diffusivity of semitransparent solids, *Meas. Sci. Technol.* 25(3) (2014), art. no. 035604.
DOI: [10.1088/0957-0233/25/3/035604](https://doi.org/10.1088/0957-0233/25/3/035604)